Functional Specialization of Cellulose Synthase Isoforms in a Moss Shows Parallels with Seed Plants[1][OPEN]

Joanna H. Norris,[a] Xingxing Li,[a] Shixin Huang,[b] Allison M. L. Van de Meene,[c] Mai L. Tran,[a] Erin Killeavy,[a] Arielle M. Chaves,[a] Bailey Mallon,[a,2] Danielle Mercure,[a,3] Hwei-Ting Tan,[d,4] Rachel A. Burton,[d] Monika S. Doblin,[c] Seong H. Kim,[b] and Alison W. Roberts[a,5]

[a]Department of Biological Sciences, University of Rhode Island, Kingston, Rhode Island 02881
[b]Department of Chemical Engineering, Pennsylvania State University, University Park, Pennsylvania 16802
[c]Australian Research Council Centre of Excellence in Plant Cell Walls, Plant Cell Biology Research Centre, School of BioSciences, University of Melbourne, Melbourne, Victoria 3010, Australia
[d]Australian Research Council Centre of Excellence in Plant Cell Walls, School of Agriculture, Food, and Wine, University of Adelaide, Waite Campus, Glen Osmond, South Australia 5064, Australia

ORCID IDs: 0000-0002-6521-5462 (J.H.N.); 0000-0002-4567-6712 (A.M.C.); 0000-0002-9332-6530 (B.M.); 0000-0002-2006-1439 (H.-T.T.); 0000-0002-8921-2725 (M.S.D.); 0000-0002-8575-7269 (S.H.K.); 0000-0002-7775-5589 (A.W.R.).

The secondary cell walls of tracheary elements and fibers are rich in cellulose microfibrils that are helically oriented and laterally aggregated. Support cells within the leaf midribs of mosses deposit cellulose-rich secondary cell walls, but their biosynthesis and microfibril organization have not been examined. Although the *Cellulose Synthase* (*CESA*) gene families of mosses and seed plants diversified independently, *CESA* knockout analysis in the moss *Physcomitrella patens* revealed parallels with Arabidopsis (*Arabidopsis thaliana*) in CESA functional specialization, with roles for both subfunctionalization and neofunctionalization. The similarities include regulatory uncoupling of the CESAs that synthesize primary and secondary cell walls, a requirement for two or more functionally distinct CESA isoforms for secondary cell wall synthesis, interchangeability of some primary and secondary CESAs, and some CESA redundancy. The cellulose-deficient midribs of *ppcesa3/8* knockouts provided negative controls for the structural characterization of stereid secondary cell walls in wild type *P. patens*. Sum frequency generation spectra collected from midribs were consistent with cellulose microfibril aggregation, and polarization microscopy revealed helical microfibril orientation only in wild type leaves. Thus, stereid secondary walls are structurally distinct from primary cell walls, and they share structural characteristics with the secondary walls of tracheary elements and fibers. We propose a mechanism for the convergent evolution of secondary walls in which the deposition of aggregated and helically oriented microfibrils is coupled to rapid and highly localized cellulose synthesis enabled by regulatory uncoupling from primary wall synthesis.

In vascular plants, cellulose is a major component of both primary cell walls, which are deposited during cell expansion, and secondary cell walls, which are deposited after expansion has ceased (Carpita and McCann, 2000). Secondary cell walls of water-conducting tracheary elements and supportive fibers are rich in cellulose, with microfibrils arranged in helices that vary in angle according to developmental stage and environmental conditions (Barnett and Bonham, 2004). Secondary cell wall microfibrils also are more aggregated than those of primary cell walls (Donaldson, 2007; Fernandes et al., 2011; Thomas et al., 2014). Recently, sum frequency generation (SFG) spectroscopy has been used to compare the mesoscale structure of cellulose microfibrils in primary and secondary cell walls. Both high cellulose content and microfibril aggregation contribute to a strong secondary cell wall signature in SFG spectra of mature angiosperm tissues (Barnette et al., 2012; Park et al., 2013; Lee et al., 2014).

Cellulose microfibrils are synthesized by cellulose synthase (CESA) proteins that function together as cellulose synthesis complexes (CSCs) in the plasma membrane (Delmer, 1999; Kimura et al., 1999). Recent analyses of CSC and microfibril structure indicate that the rosette CSCs of land plants most likely contain 18 CESA subunits (Fernandes et al., 2011; Jarvis, 2013; Newman et al., 2013; Thomas et al., 2014; Oehme et al., 2015; Nixon et al., 2016; Vandavasi et al., 2016) in a 1:1:1 ratio (Gonneau et al., 2014; Hill et al., 2014). Seed plants have six phylogenetic and functional classes of CESA proteins, three required for primary cell wall synthesis (Desprez et al., 2007; Persson et al., 2007) and three required for the synthesis of the lignified secondary cell walls of tracheary elements and fibers (Taylor et al., 2003). Mutation of any of the secondary CESAs results in a distinctive irregular xylem phenotype characterized by collapsed xylem tracheary elements and weak stems (Taylor et al., 2004). The secondary cell wall CESAs of Arabidopsis (*Arabidopsis thaliana*) are regulated by master regulator NAC domain transcription factors that also activate genes required for the synthesis of other secondary cell wall components,

such as xylan and lignin (Schuetz et al., 2013; Zhong and Ye, 2015; Yang and Wang, 2016).

The moss *Physcomitrella patens* has seven *CESA* genes (Roberts and Bushoven, 2007; Goss et al., 2012). Phylogenetic analysis has revealed that the *P. patens* CESAs do not cluster with the six CESA clades shared by seed plants (Roberts and Bushoven, 2007). Like other mosses, *P. patens* lacks the lignified secondary cell walls that are characteristic of vascular plant tracheary elements and fibers. However, mosses do have support cells (stereids) with thick unlignifed cell walls (Kenrick and Crane, 1997) and water-conducting cells (hydroids) that have thin cell walls and undergo programmed cell death like tracheary elements (Hebant, 1977). Although the stereid cell walls of *P. patens* are known to contain cellulose (Berry et al., 2016), the mesoscale structure has not been examined. Only one of the seven *P. patens* CESAs has been characterized functionally. When *PpCESA5* was disrupted, gametophore buds failed to develop into leafy gametophores, instead forming irregular cell clumps. The associated disruptions of cell expansion and cell division are consistent with an underlying defect in primary cell wall deposition (Goss et al., 2012). Recently it was shown that *PpCESA3* expression is regulated by the NAC transcription factor *PpVNS7*, along with the thickening of stereid cell walls (Xu et al., 2014).

Here, we show that PpCESA3 and PpCESA8 function in the deposition of stereid cell walls in the gametophore leaf midribs of *P. patens* and are subfunctionalized with respect to PpCESA5. We also used polarization microscopy and SFG to reveal similarities in the mesoscale organization of the microfibrils synthesized by PpCESA3 and PpCESA8 and those in the secondary cell walls of vascular plants. Finally, we propose a mechanism through which the uncoupling of primary and secondary CESA regulation played a role in the independent evolution of secondary cell walls with aggregated, helically arranged cellulose microfibrils in the moss and seed plant lineages.

RESULTS

PpCESA3 and PpCESA8 Function in Secondary Cell Wall Deposition

The CESA genes *PpCESA3* and *PpCESA8* were independently knocked out by homologous recombination in an effort to examine their roles in development and cell wall biosynthesis in *P. patens*. Stable antibiotic-resistant lines generated by transforming wild type *P. patens* with CESA3KO or CESA8KO vectors were tested for integration of the vector and deletion of the target gene by PCR (Supplemental Fig. S1). Integration was verified for five *ppcesa8*KO lines recovered from two different transformations, line 8KO-5B from a transformation of the GD06 wild type line and lines 8KO-4C, 8KO-5C, 8KO-7C, and 8KO-10C from a transformation of the GD11 wild type line (Supplemental Fig. S1). Integration was verified for three *ppcesa3*KO lines recovered from a single transformation of GD11 and three double *ppcesa3/8*KO lines recovered from a single transformation of the *ppcesa8*KO-5B line with the CESA3KO vector (Supplemental Fig. S1). The GD06 and GD11 lines are from independent selfings of the same haploid wild type line, as described in "Materials and Methods."

The colonies that developed from wild type and KO lines consisted of protonemal filaments and leafy gametophores (Fig. 1). Whereas wild type, *ppcesa3*KO, and *ppcesa8*KO gametophores grew vertically, the gametophores on *ppcesa3/8*KO colonies were unable to support themselves and adopted a horizontal orientation. Superficially, *ppcesa3/8*KO colonies appeared to produce fewer gametophores (Fig. 1), but dissection revealed similar numbers of horizontal gametophores that had been overgrown by protonemal filaments. Thus, PpCESA3 and PpCESA8 are not required for gametophore initiation or morphogenesis, but they appear to contribute to structural support.

When examined with polarized light microscopy, the wild type gametophore leaves exhibited strong cell wall birefringence in the midribs and margins (Fig. 1). In contrast, the leaves produced by *ppcesa3/8*KOs lacked strong birefringence in these cells, consistent with the

[1] This work was supported primarily by National Science Foundation Award IOS-1257047. Analysis of mutants by SFG spectroscopy was supported as part of the Center for LignoCellulose Structure and Formation, an Energy Frontier Research Center funded by the U.S. Department of Energy, Office of Science, Office of Basic Energy Sciences Award DE-SC0001090. CBM3a affinity cytochemistry and freeze substitution transmission electron microscopy were supported by the Australian Research Council Centre for Excellence in Plant Cell Walls Grant CE1101007. High-pressure freezing and transmission electron microscopy were undertaken at the Melbourne Advanced Microscopy Facility at the Bio21 Institute and the Biosciences Microscopy Unit at the University of Melbourne. DNA sequencing and qPCR were conducted using the Rhode Island Genomics and Sequencing Center, a Rhode Island National Science Foundation EPSCoR research facility, supported in part by the National Science Foundation EPSCoR Cooperative Agreement EPS-1004057.

[2] Current address: Neuroimaging Research Branch, National Institutes of Health, Baltimore, MD 21224.

[3] Current address: Pfizer, Inc., Groton, CT 06340.

[4] Current address: Centre for Tropical Crops and Biocommodities, Queensland University of Technology, Brisbane, Queensland 4000, Australia.

[5] Address correspondence to aroberts@uri.edu.

The author responsible for distribution of materials integral to the findings presented in this article in accordance with the policy described in the Instructions for Authors (www.plantphysiol.org) is: Alison W. Roberts (aroberts@uri.edu).

J.H.N. and A.W.R. conceived the project and supervised and performed experiments; X.L., S.H., A.M.L.V.d.M., and M.L.T. designed and performed experiments and analyzed the data; A.M.C., E.K., B.M., D.M., and H.-T.T. performed experiments; S.H.K. supervised experiments; A.W.R. wrote the article with contributions from J.H.N., S.H., A.M.L.V.d.M., S.H.K., R.A.B., and M.S.D; all authors read and approved the article.

[OPEN] Articles can be viewed without a subscription.

www.plantphysiol.org/cgi/doi/10.1104/pp.17.00885

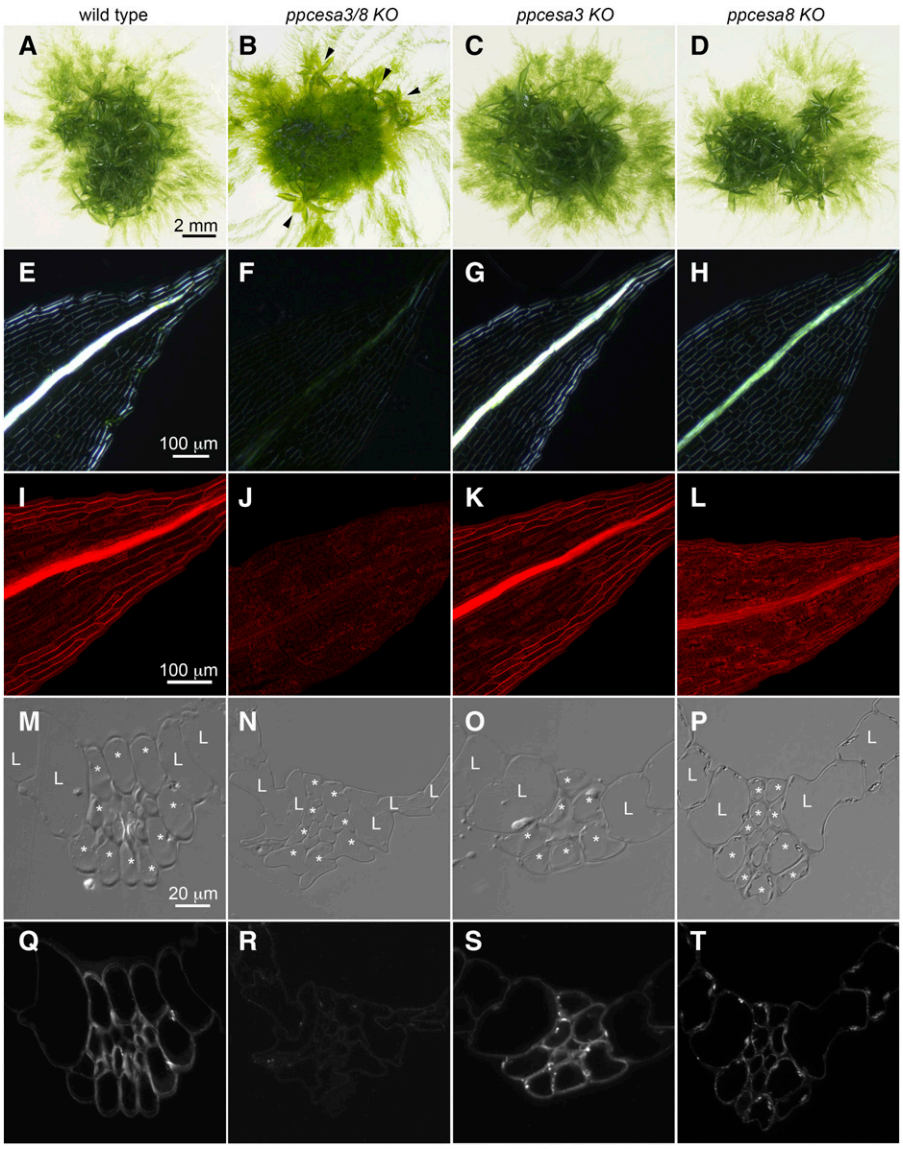

Figure 1. Phenotypes of *ppcesa3/8*KO, *ppcesa3*KO, and *ppcesa8*KO compared with wild type *P. patens*. A to D, Colony morphology is similar in the wild type, *ppcesa3*KOs, and *ppcesa8*KOs; horizontal growth is typical of gametophores produced by *ppcesa3/8*KO (arrowheads). E to H, Polarized light microscopy of leaves shows that the midribs of the wild type and *ppcesa3*KO are highly birefringent. The midribs of *ppcesa3/8*KO leaves have low birefringence, and *ppcesa8*KO midribs have moderate birefringence. I to L, Fluorescence microscopy of leaves stained with Pontamine Fast Scarlet (S4B) shows strong fluorescence in the midribs of wild type and *ppcesa3*KO leaves, low fluorescence in the midribs of *ppcesa3/8*KO leaves, and intermediate fluorescence in the midribs of *ppcesa8*KO leaves. M to P, Differential interference contrast microscopy of sections through the midribs of maturing leaves (L, lamina cell; *, bundle sheath cell). In the wild type and *ppcesa3*KO, the walls of bundle sheath cells and the stereid cells they surround show enhanced contrast due to differential refractive index. Q to T, Fluorescence microscopy of the same sections shown in M to P labeled with CBM3a. The bundle sheath and stereid cells of wild type and *ppcesa3*KO leaves are strongly labeled, whereas labeling is weak in *ppcesa3/8*KO and intermediate in *ppcesa8*KO leaves.

reduced crystalline cellulose content. The *ppcesa3*KO leaves appeared similar to wild type leaves (Fig. 1), and *ppcesa8*KO leaves had an intermediate phenotype. Staining with the fluorescent cellulose-binding dye S4B (Anderson et al., 2010) produced similar results, with strong fluorescence in the midribs of wild type and *ppcesa3*KO leaves, weak fluorescence in *ppcesa3/8*KO leaves, and intermediate fluorescence in *ppcesa8*KO leaves (Fig. 1).

Carbohydrate Binding Module 3a (CBM3a) provides a third method for detecting cellulose and can be used to probe thin sections (Blake et al., 2006). In sections from fully expanded wild type leaves, the walls of the lamina cells were labeled relatively weakly with CBM3a, whereas the thickened cell walls of the central midrib and bundle sheath cells were strongly labeled (Fig. 1). The same was true for *ppcesa3*KO leaves. However, midrib and bundle sheath cell labeling was nearly absent in *ppcesa3/8*KO and diminished in *ppcesa8*KO (Fig. 1) compared with the wild type and *ppcesa3*KO. Differential interference contrast microscopy of the same sections showed enhanced contrast in wild type and *ppcesa3*KO midribs (Fig. 1). Partial cell collapse occurred during embedding in *ppcesa3/8*KO leaves (Fig. 1).

The cellulose content of the leaf midribs in the wild type and single and double *ppcesa*KO mutants was quantified by measuring the intensity of S4B fluorescence. Statistical analysis confirmed that the S4B fluorescence was reduced significantly in double KOs but not in *ppcesa3*KOs (Fig. 2). The intermediate phenotype of the *ppcesa8*KOs was confirmed and shown to be significantly different from both the wild type and the double KOs (Fig. 2). Updegraff analysis showed that the cellulose content of cell walls from whole *ppcesa3/8*KO gametophores (mean ± SE of three genetic

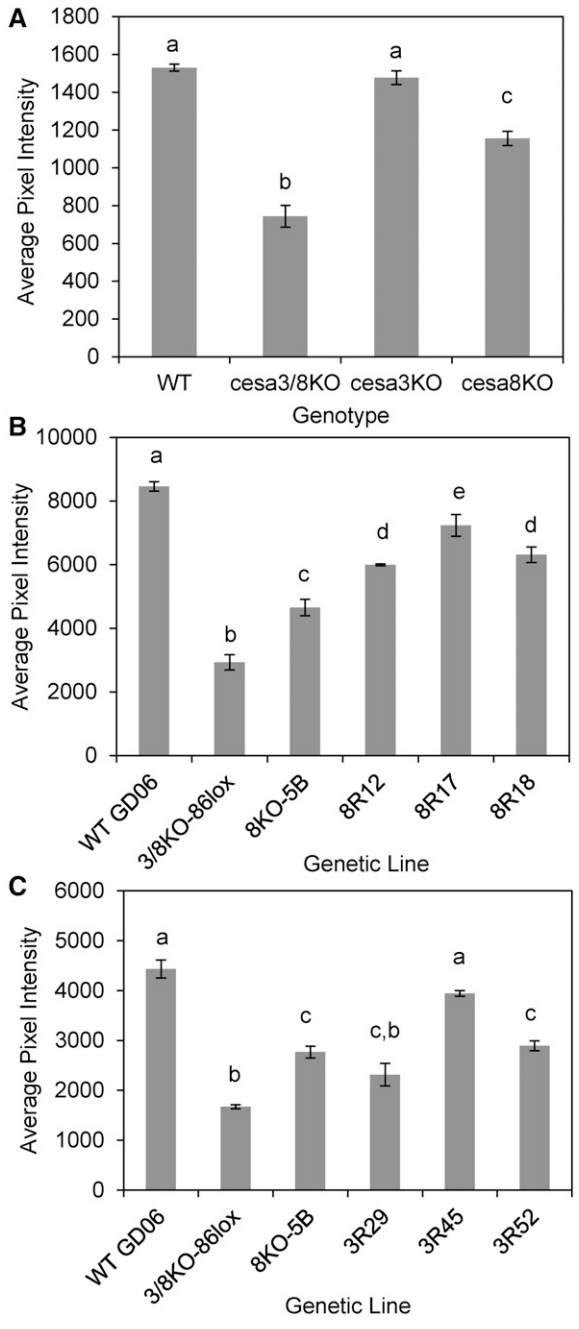

Figure 2. Quantitative analysis of S4B fluorescence intensity in leaf midribs of *P. patens* wild type (WT), *ppcesa*KO, and rescue lines. Genotypes with different letters are significantly different ($P < 0.05$). A, Fluorescence was significantly weaker in *ppcesa3/8*KOs compared with the wild type. *ppcesa3*KOs were not significantly different from the wild type, whereas *ppcesa8*KOs were intermediate between the wild type and *ppcesa3/8*KOs and significantly different from both. For each mutant genotype, three independent genetic lines were sampled in triplicate. Two independent wild type lines (GD06 and GD11) were sampled in triplicate. Error bars indicate SE for three mutant ($n = 3$) or two wild type ($n = 2$) lines. B, Lines derived from transformation of *ppcesa3/8*KO-86lox with *proCESA8*::*CESA8* (8R) had significantly higher fluorescence compared with the parent double KO line and *ppcesa8*KO but significantly less than the wild type. C, Lines derived from transformation of *ppcesa3/8*-86lox with *proCESA3*::*CESA3* (3R) had significantly higher fluorescence compared with the parent double KO line (except 3R29) and were not significantly different from either *ppcesa8*KO lines (3R29 and 3R52) or the wild type (3R45). For B and C, error bars indicate SE for explants from the same line ($n = 3$ or $n = 2$ [WT, 3/8KO, and 8KO in C]).

lines = 33.8% ± 0.034%) was reduced significantly ($P = 0.004$) compared with the wild type (GD06; mean ± SE of three independent cultures = 60.1% ± 0.030%).

To confirm that the observed *ppcesa3/8*KO phenotype was due to the absence of PpCESA3 and PpCESA8, the selection cassette was removed from *ppcesa3/8*KO-86 by Cre-mediated recombination of flanking *lox-p* sites (Vidali et al., 2010) to allow transformation with vectors that drive the expression of PpCESA3 or PpCESA8 with their native promoters (Supplemental Fig. S2). Stable antibiotic-resistant lines selected for the presence of numerous erect gametophores were examined with polarization microscopy (Supplemental Fig. S2). For the transformation with *proCESA8*::*CESA8*, 13 lines were examined, six of these had strong midrib birefringence, and the first three were used for further analysis. For the transformation with *proCESA3*::*CESA3*, the first three lines examined had strong midrib birefringence and were used for further analysis. S4B staining confirmed that expression of PpCESA8 or PpCESA3 rescued the defects in cellulose deposition in the leaf midribs of the double *ppcesa3/8*KO (Fig. 2). Lines from the transformation with *proCESA8*::*CESA8* were expected to be restored to the wild type phenotype, because *ppcesa3*KO, which also expresses *PpCESA8* under the control of the *PpCESA8* promoter, showed no defects in cellulose deposition in the leaf midrib. All three *proCESA8*::*CESA8* lines had significantly stronger S4B fluorescence than *ppcesa8*KO. This demonstrates substantial restoration of the phenotype, although fluorescence was still significantly weaker than in the wild type (Fig. 2). Two lines from a transformation with *proCESA3*::*CESA3* (3R29 and 3R52) were not significantly different from *ppcesa8*KO-5B, which is expected, since they both lack *PpCESA8* and express *PpCESA3* under the control of the *PpCESA3* promoter. In the third line (3R45), fluorescence was restored to wild type levels (Fig. 2). The *y* axis scales differ between experiments due to the use of different exposure time settings.

Secondary Cell Wall Microfibrils Are Helically Oriented and Laterally Aggregated

A first-order retardation plate was used with polarized light microscopy to determine the optical sign, and thus the cellulose microfibril orientation, of wild type and *ppcesa3/8*KO midrib cell walls (Fig. 3). In mature wild type leaves, the larger bundle sheath-like cells that surround the central stereids showed blue addition colors when oriented parallel to the major axis of the plate and yellow subtraction colors when oriented

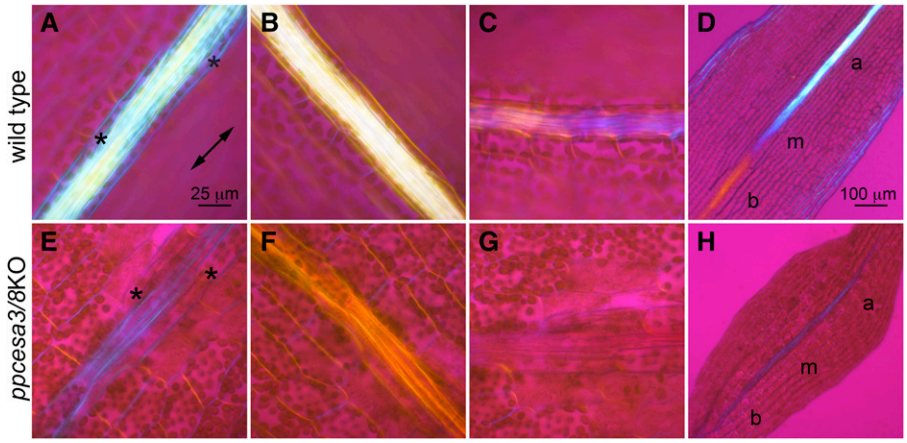

Figure 3. Polarized light microscopy with a first-order retardation plate. The double-pointed arrow indicates the vibration direction of the major axis. A to C, Midrib of a mature wild type leaf oriented parallel, perpendicular, and at 45° to the major axis of the retardation plate. Bundle sheath cells (asterisks) flank the central midrib. D, Midrib of a developing wild type leaf oriented parallel to the major axis of the retardation plate showing change in microfibril orientations through the basal (b), medial (m), and apical (a) regions of the midrib. E to G, Midrib of a mature *ppcesa3/8*KO leaf oriented parallel, perpendicular, and at 45° to the major axis of the retardation plate. H, Midrib of a developing *ppcesa3/8*KO leaf oriented parallel to the major axis of the retardation plate showing no change in microfibril orientation through the basal, medial, and apical regions of the leaf. Bar in A is also for B, C, and E to G, and bar in D is also for H.

perpendicular to the major axis (Fig. 3), indicating that the net orientation of positively birefringent cellulose microfibrils is longitudinal. In contrast, the walls of the smaller central stereids were colorless when oriented parallel or perpendicular to the major axis (Fig. 3). However, when oriented at 45° to the retardation plate, these cells showed alternating bands of blue and yellow (Fig. 3), indicating that the microfibrils in their walls are helical with an angle near 45°. The central midrib cells of developing wild type leaves showed a transition from colorless to blue to yellow along the apical to basal developmental gradient when the midrib was oriented parallel to the major axis of the plate (Fig. 3). This indicates that the microfibril orientation changes from transverse to longitudinal and then to helical as the cells mature. In contrast, the central midrib stereids of mature *ppcesa3/8*KO leaves had blue addition colors when oriented parallel to the major axis, yellow subtraction colors when oriented perpendicular to the major axis, and no interference color when oriented at 45° to the retardation plate, indicating that microfibrils are longitudinal rather than helical. Developing *ppcesa3/8*KO leaves had no longitudinal gradient in interference colors (Fig. 3).

The walls of midrib cells were examined by transmission electron microscopy in ultrathin sections of chemically fixed gametophore leaves. Despite the reduced cellulose content detected by other means, the walls of midrib cells were thickened compared with the walls of adjacent lamina cells in all *ppcesa*KOs as well as wild type leaves (Fig. 4). When we attempted to prepare specimens by high-pressure freezing and freeze substitution, the leaves fractured in a plane parallel to the midrib. This resulted in a loss of midrib cells and precluded the examination of midrib cell walls in these specimens. We were able to examine the lamina and margin cells of freeze-substituted leaves in the wild type and two lines of each mutant. The walls of these cells appeared similar between the wild type and single and double *ppcesa*KOs (Supplemental Fig. S3). However, measurements revealed that lamina

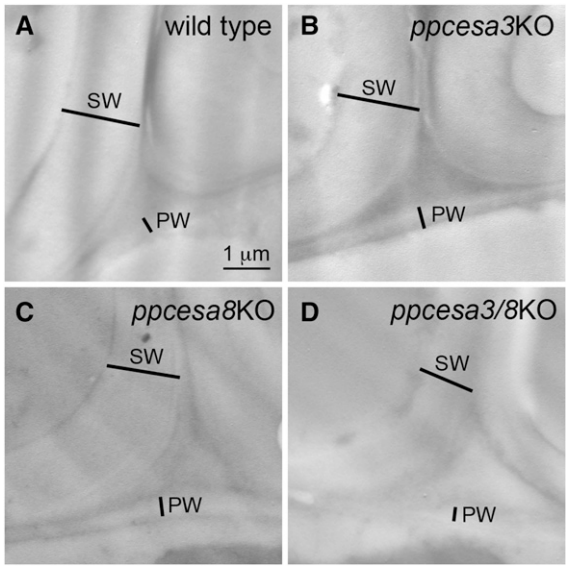

Figure 4. Transmission electron microscopy images of leaf midribs of *P. patens* showing adjacent cells with primary cell walls (PW) and secondary cell walls (SW) in wild type (A) and mutant (B–D) leaves.

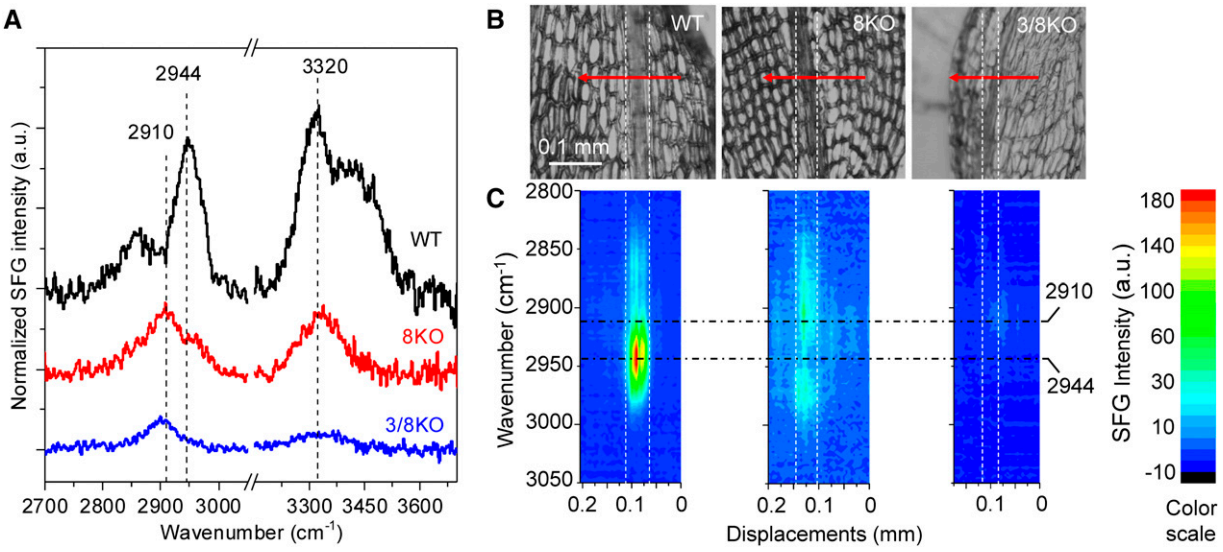

Figure 5. SFG spectroscopy of *P. patens* leaves. A, Full SFG spectra collected from leaf midribs (each is the average of nine spectra from three different positions on each of three different leaves). A strong peak in the CH stretch region (2,944 cm^{-1}) is present in spectra from the wild type (WT), greatly diminished in spectra from *ppcesa8*KO (8KO), and absent in spectra from *ppcesa3/8*KO (3/8KO). B, *P. patens* wild type, *ppcesa8*KO, and *ppcesa3/8*KO leaves with SFG scan trajectories traversing the midribs. Step size was 5 μm per step. SFG spectra were collected from 2,850 to 3,150 cm^{-1}, covering the entire CH region. C, 2D projection image of SFG spectra collected across the midribs of each leaf shown in B. Each column in each image is an entire spectrum collected from one point plotted against displacement along the scan trajectory. Colors indicate SFG intensity as shown in the scale at right.

cell external walls (i.e. those facing the external environment) were thinner in *ppcesa*KOs (Supplemental Fig. S4).

The mesoscale organization of cellulose in the midribs of wild type, *ppcesa3/8*KO, and *ppcesa8*KO leaves was examined using a broadband SFG microscope (Lee et al., 2016). Because it detects only the noncentrosymmetric ordering of functional groups, SFG provides a means of analyzing cellulose in intact cell walls with relatively little interference from matrix components (Barnette et al., 2011). For each genotype, full SFG spectra collected from three different locations along the midribs of each of three different leaves were averaged (Fig. 5). The sampling depth of the SFG microscope for cellulosic samples is 20 to 25 μm (Lee et al., 2016). Given that the thickness of turgid leaves is about 50 to 60 μm at the midrib and that they likely collapse to less than half their thickness when dried, we conclude that most of the leaf thickness contributes to the SFG signal. In spectra collected from the wild type, a strong peak at 2,944 cm^{-1}, which is characteristic of secondary cell walls, was observed in the CH/CH_2 stretch region along with a 3,320 cm^{-1} peak in the OH stretch region. In contrast, the spectra collected from *ppcesa3/8*KO and *ppcesa8*KO midribs had weaker peak intensity overall, with a broad CH/CH_2 stretch peak centered around 2,910 cm^{-1}. Compared with *ppcesa3/8*KO, the spectra from *ppcesa8*KO midribs had a weak signal at 2,963 cm^{-1} that was absent in spectra collected from *ppcesa3/8*KO midribs. A scan across a wild type leaf shows that the 2,944 cm^{-1} signal is associated with the midrib and was not observed in the cells of the lamina (Fig. 5). Equivalent scans of *ppcesa3/8*KO and *ppcesa8*KO leaves confirm the absence of a strong 2,944 cm^{-1} peak from the midribs of these mutants (Fig. 5).

PpCESA Proteins Are Functionally Specialized

Based on the *ppcesa3*KO, *ppcesa8*KO, and *ppcesa3/8*KO phenotypes, PpCESA3 and PpCESA8 appear to be partially redundant. To determine whether the relative strengths of these phenotypes are related to gene expression levels, we used reverse transcription quantitative PCR to measure the expression of *PpCESA3* and *PpCESA8* in the wild type and mutants. In the *ppcesa3*-KOs, *PpCESA8* was up-regulated significantly compared with the wild type (Fig. 6), providing a possible explanation for the lack of a mutant phenotype in these lines. In contrast, *PpCESA3* was not up-regulated significantly in *ppcesa8*KOs compared with the wild type, potentially explaining the intermediate phenotype in these mutants.

*ppcesa3*KOs, *ppcesa8*KOs, and *pp*cesa3/*8*KOs were tested for changes in rhizoid and caulonema development to determine whether developmental defects were restricted to the gametophores. When cultured on medium containing auxin, all lines produced the expected leafless gametophores with numerous rhizoids (Supplemental Fig. S5), indicating no defects in rhizoid development in any of the KOs. Caulonema produced by colonies grown in the dark on vertically oriented plates were all negatively gravitropic (Supplemental Fig. S6). Although the appearance of the caulonema

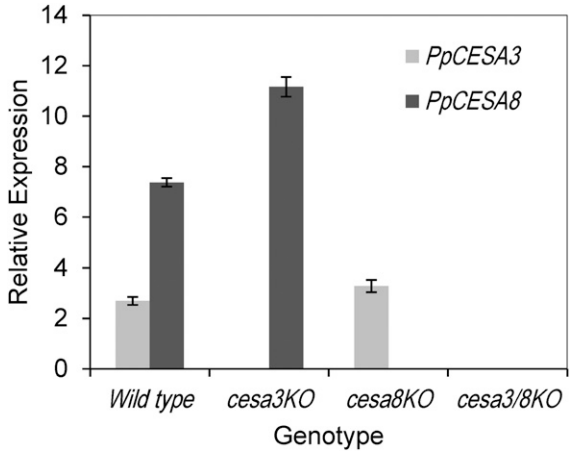

Figure 6. Reverse transcription quantitative PCR analysis of *PpCESA3* and *PpCESA8* expression in the wild type, *ppcesa3*KOs, and *ppcesa8*-KOs. Target/average reference cross-point ratios (using actin and v-type H^+-translocating pyrophosphatase reference genes) were determined for three independent lines of each mutant (3KO-5, 3KO-35, 3KO-126; 8KO-5B, 8KO-4C, 8KO-10C; and 3/8KO-43, 3/8KO-57, 3/8KO-86) and two independent wild type lines (GD06 and GD11) with two technical replicates each. Error bars indicate SE for the three mutant ($n = 3$) or two wild type ($n = 2$) lines.

varied among experiments, those produced by KOs were always similar to the control wild type within the same experiment. Caulonemal length was not significantly different between *ppcesa3/8*KOs and the wild type (Table I).

To determine whether other PpCESAs are functionally interchangeable with PpCESA3 and PpCESA8, we tested for rescue of *ppcesa3/8*KO-86lox by various *PpCESA*s driven by the *PpCESA8* promoter. Polarization microscopy screening of at least 21 and up to 27 stably transformed lines for each vector revealed little or no midrib birefringence for the *proCESA8*::*CESA4*, *proCESA8*::*CESA7*, and *proCESA8*::*CESA10* lines and moderate to strong midrib birefringence for 92% and 78% of the *proCESA8*::*CESA3* and *proCESA8*::*CESA5* lines, respectively. Quantitative analysis of S4B staining (Fig. 7) confirmed that the *ppcesa3/8*KO phenotype was partially rescued by *proCESA8*::*CESA3* (three out of three lines) and *proCESA8*::*CESA5* (two out of three lines), as we observed for *proCESA8*::*CESA8* (Fig. 2). However, the *proCESA8*::*CESA4*, *proCESA8*::*CESA7*, and *proCESA8*::*CESA10* vectors showed no rescue (Fig. 7). Western-blot analysis confirmed that PpCESA proteins were expressed in all lines except *proCESA8*::*CESA4*-11 and *proCESA8*::*CESA5*-7 (Supplemental Fig. S7). PpCESA6 differs from PpCESA7 by only two amino acids and was not tested. Although expressed with the same promoter, protein accumulation varies among the different transgenic lines (Supplemental Fig. S7). Similar differences in protein accumulation also may explain the variation in the extent of rescue by the *proCESA3*::*CESA3* and *proCESA8*::*CESA8* vectors (Fig. 2).

Finally, we examined *ppcesa4/10*KOs and *ppcesa6/7*KOs produced for another study to determine whether they phenocopy the *ppcesa3/8*KO phenotype. Genotype verification for these lines is presented in Supplemental Figures S8 and S9. The *ppcesa4/10*KOs showed slight but significant reduction in midrib S4B fluorescence. However, for *ppcesa6/7*KOs, the reduction was substantial and significant (Fig. 7), showing the PpCESA6/7 and PpCESA3/8 have nonredundant roles in secondary cell wall deposition in leaf midrib cells.

DISCUSSION

PpCESA3 and PpCESA8 Function Redundantly in Cellulose Deposition in Stereid Secondary Cell Walls

Targeted knockout of *PpCESA3* and *PpCESA8* blocked the deposition of cellulose in the thick walls of stereid cells, as indicated by (1) reduction of the strong birefringence associated with the midribs in *ppcesa3/8*KOs, (2) reduction in the midrib fluorescence of *ppcesa3/8*KO leaves stained with S4B, (3) lack of CBM3a labeling of sections from *ppcesa3/8*KO leaf midribs (Fig. 1), and (4) reduction in *ppcesa3/8*KO gametophore cell wall cellulose content as measured by Updegraff assay. Evidence that knockout of *PpCESA3* and *PpCESA8* is responsible for the observed phenotype includes the consistency of the phenotype in three independent KOs and the restoration of cellulose deposition in the midribs by the transformation of *ppcesa3/8*KO with vectors driving the expression of PpCESA3 or PpCESA8 (Fig. 2). Whereas we detected no reduction in midrib cellulose in *ppcesa3*KOs, the phenotypes of *ppcesa8*KOs were intermediate between the wild type and *ppcesa3/8*KO (Fig. 2). This, combined with the observations that only *PpCESA8* is up-regulated to compensate for the loss of its paralog (Fig. 6) and the expression of PpCESA3 under the control of its native promoter only partially restores the wild type phenotype (Fig. 2), is consistent with the hypothesis that the PpCESA3 and PpCESA8 proteins are functionally interchangeable and that a dosage effect is responsible for the *ppcesa8*KO phenotype. The formation of morphologically normal gametophores in *ppcesa3/8*KOs (Fig. 1) indicates that PpCESA3 and PpCESA8 serve a different role in development than PpCESA5, which supports the normal cell division and cell expansion required for gametophore development (Goss et al., 2012). It is possible that PpCESA3 and PpCESA8 contribute to primary cell wall

Table I. *Caulonema length for the wild type and ppcesa3/8KOs grown on vertical plates in the dark*

Data are from two independent experiments ($n = 2$). ANOVA showed no significant differences between genetic lines.

Genetic Line	Caulonema Length	SE
	mm	
Wild type GD06	4.69	0.50
*ppcesaA3/8*KO-43	5.70	0.87
*ppcesaA3/8*KO-57	4.51	1.14
*ppcesaA3/8*KO-86	5.69	0.47

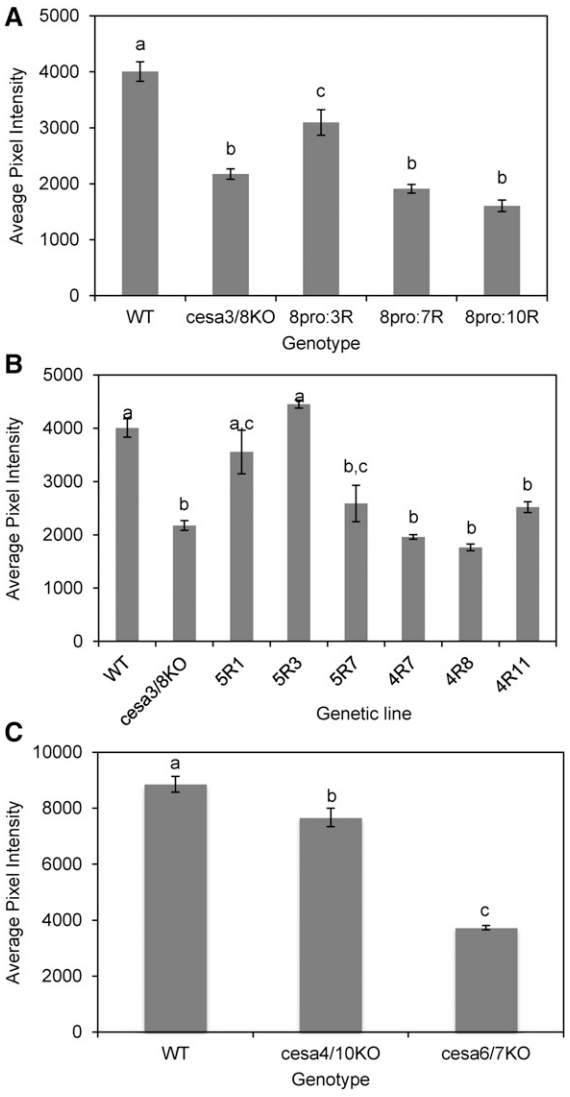

Figure 7. Quantitative analysis of S4B fluorescence intensity in leaf midribs. A and B, Wild type (WT), *ppcesa3/8*KO-86lox, and *ppcesa3/8*KO-86lox transformed with *proCESA8*::*CESA* expression vectors. For each rescue genotype, three independent genetic lines were sampled in triplicate and measured with six samples of the wild type (GD06) and eight samples of *ppcesa3/8*KO-86lox. A, For lines derived from transformation of *ppcesa3/8*KO-86lox with *proCESA8*::*CESA3* (8pro:3R), *proCESA8*::*CESA7* (pro8:7R), and *proCESA8*::*CESA10* (pro8:10R) genotypes, the three independent lines did not differ significantly and were combined. *proCESA8*::*CESA7* and *proCESA8*::*CESA10* lines did not differ significantly from the parent double KO line ($P > 0.05$), whereas *proCESA8*::*CESA3* lines had significantly higher fluorescence compared with the parent double KO line but significantly less than the wild type ($P < 0.05$). Error bars indicate SE for three independent lines. Genotypes with different letters are significantly different ($P < 0.05$). B, For lines derived from transformation of *ppcesa3/8*KO-86lox with *proCESA8*::*CESA5* (pro8:5R) and *proCESA8*::*CESA4* (pro8:4R), the three independent lines were significantly different and were analyzed separately. *proCESA8*::*CESA5* (5R) lines were not significantly different from the wild type ($P > 0.05$), except for 5R7, which was not significantly different from *ppcesa3/8*KO-86lox ($P > 0.05$). *proCESA8*::*CESA4* lines did not differ significantly from *ppcesa3/8*KO-86lox ($P > 0.05$). Error bars indicate SE for three gametophores from the same line ($n = 3$). Lines with different letters are significantly different ($P < 0.05$). C, Midrib fluorescence was slightly but significantly reduced in *cesa4/10*KO compared with the wild type ($P = 0.037$). Reduction in midrib fluorescence in *cesa6/7*KO was substantial and highly significant ($P = 0.0011$). Error bars indicate SE for three independent mutant lines or three replicates of the wild type ($n = 3$). Genotypes with different letters are significantly different ($P < 0.05$).

deposition, since *ppcesa3/8*KO lamina cells had thinner external walls (Supplemental Fig. S4) and tended to collapse during embedding (Fig. 1). Alternatively, PpCESA3 and PpCESA8 may contribute to the secondary thickening of lamina cell walls after they stop expanding.

CESA Evolution in Both *P. patens* and Arabidopsis Involves Subfunctionalization and Neofunctionalization

There are many parallels in the evolution of the *P. patens* and Arabidopsis *CESA* families. In both species, different CESAs are responsible for primary and secondary cell wall deposition. In Arabidopsis, the secondary CESAs are AtCESA4, AtCESA7, and AtCESA8 (Taylor et al., 2003) and the primary CESAs are AtCESA1, AtCESA3, and members of the 6-like group (Desprez et al., 2007; Persson et al., 2007). In *P. patens*, midrib secondary cell wall synthesis involves PpCESA3, PpCESA6, PpCESA7, and PpCESA8, whereas gametophore primary cell wall synthesis requires PpCESA5 (Goss et al., 2012). At least some primary CESAs can substitute for secondary CESAs and vice versa in both species. In Arabidopsis, *AtCESA3pro*::*AtCESA7* partially rescues *atcesa3* and *AtCESA8pro*::*AtCESA1* partially rescues *atcesa8* (Carroll et al., 2012). In *P. patens*, *PpCESA8pro*::*PpCESA5* rescues *ppcesa3/8*KO. This indicates that the *CESA* division of labor for primary and secondary cell wall deposition in vascular plants and mosses is due at least in part to subfunctionalization. However, neofunctionalization also has occurred in both species, resulting in the requirement for two or more noninterchangeable CESA isoforms for secondary cell wall biosynthesis. In Arabidopsis, *atcesa4*, *atcesa7*, and *atcesa8* null mutants share a phenotype (Taylor et al., 2000) that cannot be complemented by expressing one of the other secondary AtCESAs with the promoter for the missing isoform (Kumar et al., 2017). Likewise in *P. patens*, *ppcesa3/8*KO and *ppcesa6/7*KO share the same phenotype, and *ppcesa3/8*KO is not complemented by *PpCESA8pro*::*PpCESA7*. Studies are ongoing to determine whether the secondary PpCESAs interact physically to form a CSC, as has been shown for the secondary AtCESAs (Taylor et al., 2003; Timmers et al., 2009). Finally, the *CESA* families of both species show some redundancy. In Arabidopsis, the 6-like *CESA*s (*AtCESA2*, *AtCESA5*, *AtCESA6*, and *AtCESA9*) are partially redundant (Persson et al., 2007), as are *PpCESA3* and *PpCESA8* in *P. patens*. PpCESA6 and PpCESA7 differ by only three amino

acids, and the genes that encode them appear to be redundant (Wise et al., 2011).

A recent study has shown that secondary cell wall deposition, including CESA expression, is regulated by NAC transcription factors in both *P. patens* and Arabidopsis (Xu et al., 2014). Three *P. patens* NAC genes, *PpVNS1*, *PpVNS6*, and *PpVNS7*, were expressed preferentially in leaf midribs, and *ppvns1/ppvns6/ppvns7*KOs were defective in stereid development. Overexpression of *PpVNS7* activated PpCESA3 (Xu et al., 2014). Phylogenetic analyses of NACs place eight PpVNS proteins within the clade that has variously been named subfamily NAC-c (Shen et al., 2009), subfamily Ic (Zhu et al., 2012), or the VNS group (Xu et al., 2014) and also includes the Arabidopsis vascular-related NACs VND6 (ANAC101), VND7 (ANA030), NST1 (ANAC043), NST2 (ANAC066), and NST3/SND1 (ANAC012). The three PpVNS proteins that regulate stereid development form a single sister clade with five other PpVNS proteins implicated also in other processes (Xu et al., 2014). Based on this phylogenetic analysis, the common ancestor of the mosses and seed plants had a single *VNS* gene, and it also had a single *CESA* gene (Roberts and Bushoven, 2007; Yin et al., 2009; Kumar et al., 2017). Both lineages now include secondary *CESA*s that are regulated by VNSs and primary *CESA*s that are not, indicating that *CESA* subfunctionalization occurred independently in mosses and seed plants.

Secondary Cell Wall Microfibrillar Texture Is Similar in Mosses and Vascular Plants

In vascular plants, both water-conducting tracheary elements and supportive fibers are characterized by helical (Barnett and Bonham, 2004) and aggregated (Donaldson, 2007; Fernandes et al., 2011; Thomas et al., 2014) cellulose microfibrils. The midribs of *P. patens* leaves include hydroid cells that transport water and stereid cells that provide support, but only the stereids have thick cell walls (Xu et al., 2014). With highly reduced cellulose in their stereid secondary cell walls, *ppcesa3/8*KOs provided a negative control for the structural characterization of secondary cell walls in wild type *P. patens*. A sharp SFG CH/CH_2 stretch peak at 2,944 cm^{-1} is characteristic of angiosperm secondary cell walls (Park et al., 2013), and extensive empirical testing has shown that this spectral feature is attributable to lateral microfibril aggregation (Lee et al., 2014). The 2,944 cm^{-1} peak also was present in SFG spectra of wild type *P. patens* midribs. In contrast, the spectra of *ppcesa3/8*KO leaf midribs lacked the 2,944 cm^{-1} peak and instead had a broad peak between 2,800 and 3,000 cm^{-1}, which is characteristic of primary cell walls and other samples lacking aggregated microfibrils (Park et al., 2013; Lee et al., 2014). This suggests that lateral aggregation of microfibrils is a common feature of the secondary cell walls of moss stereids and vascular plant tracheary elements and fibers. Polarization microscopy with a first-order retardation plate revealed that the microfibrils in the stereid cell walls are deposited in a helical pattern, as observed in secondary cell walls of tracheary elements and fibers (Barnett and Bonham, 2004). Although deficient in cellulose, the stereid cell walls of *ppcesa3/8*KOs were thickened, indicating that secondary cell wall synthesis involves the deposition of noncellulosic components, which proceeded in the absence of cellulose deposition. This also has been observed in developing tracheary elements treated with cellulose synthesis inhibitors (Taylor et al., 1992). Thus, stereid cell walls share structural characteristics with the cell walls of tracheary elements and fibers.

Mosses and Vascular Plants Have Acquired Similar Secondary Cell Walls through Convergent Evolution

Thick, cellulose-rich secondary cell walls provide added support for the aerial organs of mosses and vascular plants alike. Within these cell walls, the lateral aggregation and helical orientation of the microfibrils contribute to their strength and resilience. Although cortical microtubules play an important role in cellulose microfibril orientation, oriented cellulose deposition can occur in the absence of cortical microtubules, and it has been suggested previously that the aggregation and helical orientation of microfibrils in secondary walls are consequences of high CSC density during rapid cellulose deposition (Emons and Mulder, 2000; Lindeboom et al., 2008). Regulation at the level of CSC secretion was emphasized in this model (Emons and Mulder, 2000), but CSC density can potentially be regulated at the level of transcription.

Rapid cellulose synthesis during secondary cell wall deposition in specific cell types requires precise temporal and spatial regulation of CESA expression that is distinct from the regulatory requirements for primary cell wall synthesis. We suggest that these distinct regulatory needs were met through the evolution of independent regulatory control of primary and secondary CESAs by subfunctionalization in both mosses and seed plants. In seed plants, phylogenetic analysis shows that the first divergence of the *CESA* family separated the genes that encode the primary and secondary CESAs and was followed by independent diversification within each group (Roberts et al., 2012). This, along with evidence that some primary CESAs are interchangeable with secondary CESAs (Carroll et al., 2012), indicates that subfunctionalization was an early event in the evolution of the seed plant CESA family. In *P. patens*, the genes that encode secondary PpCESA3 and PpCESA8 and primary PpCESA5 are also subfunctionalized and, therefore, specialized, although they encode interchangeable proteins.

Several lines of evidence indicate that the capacity to deposit a secondary cell wall evolved independently in mosses and seed plants. Structural and paleobotanical evidence suggests that the support and water-conducting cells of bryophytes and vascular plants are not homologous (Ligrone et al., 2002; Carafa et al., 2005). Phylogenetic evidence indicates that the primary and secondary CESAs diversified independently in mosses and seed plants

(Roberts and Bushoven, 2007; Yin et al., 2009; Kumar et al., 2017) and, as explained above, so did the NAC transcription factors that regulate the secondary CESAs. There are even examples of convergent evolution of secondary cell walls within the angiosperm lineage. Cotton (*Gossypium hirsutum*) fiber secondary cell walls are synthesized by the same CESAs that are responsible for secondary cell wall deposition in tracheary elements and fibers (Haigler et al., 2012), whereas the secondary cell walls of epidermal trichomes are synthesized by the primary CESAs (Betancur et al., 2010). These observations are consistent with independent evolutionary origins for secondary cell walls in different land plant lineages and different cell types within angiosperm lineages.

Taken together, these data indicate that *CESA* duplication, followed by changes in the regulatory elements within the primary or secondary *CESA* promoters, occurred independently in mosses and vascular plants. The resulting uncoupling of the secondary CESAs from the regulatory constraints associated with primary cell wall deposition, along with a mechanistic linkage between CESA expression and microfibril texture as well as selection for strength and resilience, may have contributed to the capacity of different plants to synthesize cellulose-rich secondary cell walls with similar microfibrillar textures.

MATERIALS AND METHODS

Vector Construction

All primer pairs are shown in Supplemental Table S1, along with annealing temperatures used for PCR. Amplification programs for Taq Polymerase (New England Biolabs) consisted of a 3-min denaturation at 94°C followed by 35 cycles of 15 s at 94°C, 30 s at the annealing temperature, and 1 min kb^{-1} at 72°C. Amplification programs for Phusion Polymerase (New England Biolabs) consisted of a 30-s denaturation at 98°C followed by 35 cycles of 7 s at 98°C, 7 s at the annealing temperature, and 30 s kb^{-1} at 72°C.

To construct the CESA8KO vector, a 3′ homologous region was amplified from *Physcomitrella patens* genomic DNA with primers 174JB and 193JB using Taq DNA polymerase, cut with *Sal*I and *Bsp*DI, and cloned into the *Sal*I/*Bst*BI site of pBHSNR (a gift of Didier Schaefer, University of Neuchâtel). The resulting plasmid was cut with *Kas*I and *Nsi*I to accept the *Kas*I/*Nsi*I fragment of a 5′ homologous region amplified from *P. patens* genomic DNA with primers 203JB and 185JB (Supplemental Table S1). The CESA8KO vector was cut with *Eco*RI and *Nsi*I for transformation into wild type *P. patens*. The CESA3KO, CESA4KO, CESA6/7KO, and CESA10KO vectors were constructed using Gateway Multisite Pro cloning (Invitrogen) as described previously (Roberts et al., 2011). Flanking sequences 5′ and 3′ of the coding regions were amplified with appropriate primer pairs (Supplemental Table S1) using Phusion DNA polymerase (New England Biolabs) and cloned into pDONR 221 P1-P4 and pDONR 221 P3-P2, respectively, using BP Clonase II (Invitrogen). Similarly, an *nph* selection cassette was amplified from pMBL6 (a gift of Jesse Machuka, University of Leeds) and cloned into pDONR 221 P3r-P4r. All entry clones were sequence verified. For vectors conferring hygromycin resistance, entry clones with flanking sequences in pDONR 221 P1-P4 and pDONR 221 P3-P2 were inserted into BHSNRG (Roberts et al., 2011). For vectors conferring G418 resistance, entry clones with flanking sequences in pDONR 221 P1-P4 and pDONR 221 P3-P2 were linked with the entry clone containing the *nph* selection cassette and inserted into pGEM-gate (Vidali et al., 2009) using LR Clonase II Plus (Invitrogen). The vectors in BHSNRG or pGEM-gate were cut with *Bsr*GI for transformation into wild type or mutant *P. patens* lines.

Expression vectors for hemagglutinin (HA)-tagged PpCESAs under the control of *PpCESA* promoters were constructed using Gateway Multisite Pro cloning (Invitrogen). The *PpCESA4* (DQ902545), *PpCESA5* (DQ902546), *PpCESA7* (DQ160225), and *PpCESA8* (DQ902549) coding sequences were amplified from cDNA clones pdp21409, pdp24095, pdp38142, and pdp39044 (RIKEN BioResource Center), respectively, using forward primers containing a single HA tag and appropriate reverse primers (Supplemental Table S1) and cloned into pDONR 221 P5-P2 using BP Clonase II (Invitrogen). The *PpCESA3* (XP_001753310) and *PpCESA10* (XP_001776974) coding sequences were amplified similarly from expression vectors. pDONR 221 P1-P5r entry clones containing approximately 2 kb of sequence upstream of the *PpCESA3* or *PpCESA8* start codon (Tran and Roberts, 2016) were linked to the sequence-verified entry clones containing the *HA-PpCESA* coding sequences and inserted into pSi3(TH)GW (Tran and Roberts, 2016) using LR Clonase II Plus (Invitrogen). These vectors target the expression cassettes to the intergenic 108 locus, which can be disrupted with no effect on phenotype (Schaefer and Zrÿd, 1997). Rescue vectors were cut with *Swa*I for transformation into a *P. patens ppcesa3/8*KO line from which the *hph* resistance cassette had been removed (see below).

Culture and Transformation of *P. patens*

Wild type *P. patens* lines (haploid) derived from the sequenced Gransden strain (Rensing et al., 2008) by selfing and propagation from a single spore in 2006 (GD06) or 2011 (GD11) were gifts of Pierre-Francois Perroud (Washington University). Wild type and transformed *P. patens* lines were cultured on basal medium supplemented with ammonium tartrate (BCDAT) as described previously (Roberts et al., 2011). Protoplasts were prepared and transformed as described previously (Roberts et al., 2011). Stable transformants were selected with 50 $\mu g\ mL^{-1}$ G418 (CESA3KO vector) or 15 $\mu g\ mL^{-1}$ hygromycin (CESA8KO and complementation vectors). The *hph* selection cassette was removed from *ppces3/ppcesa8*KO by transforming protoplasts with NLS-Cre-Zeo (Vidali et al., 2010), selecting for 7 d on BCDAT plates containing 50 $\mu g\ mL^{-1}$ zeocin, replica plating zeocin-resistant colonies on BCDAT with and without 15 $\mu g\ mL^{-1}$ hygromycin, and recovering hygromycin-sensitive colonies. Protein expression was tested by western-blot analysis as described previously (Scavuzzo-Duggan et al., 2015) in selected lines transformed with HA-PpCESA expression vectors.

Genotype Analysis

For PCR screening, DNA was extracted as described previously (Roberts et al., 2011) and 2.5-μL samples were subjected to 35 cycles of amplification (45 s at 94°C, 45 s at the annealing temperature shown in Supplemental Table S1, and 1 min kb^{-1} at 72°C) with PAQ5000 DNA polymerase (Agilent Technologies) in 25-μL reactions. Primers used to test for target integration, target-gene disruption, and selection cassette excision are listed in Supplemental Table S1.

Phenotype Analysis

The cell wall birefringence of unfixed leaves mounted in water was examined using an Olympus BHS compound microscope with D Plan-Apo UV 10×/0.4, 20×/0.7, and 40×/0.85 objectives, and polarizer and circular-polarizing analyzer, with and without a first-order retardation plate (Olympus). Images were captured with a Leica DFC310FX digital camera with Leica Application Suite software, version 4.2.0 (Leica Microsystems), with manual exposure under identical conditions.

For direct fluorescent labeling of cellulose, whole gametophores (three per line) dissected from colonies grown for 4 weeks on solid BCDAT medium were dipped in 100% acetone for 5 s to permeabilize the cuticle, rinsed in phosphate-buffered saline (PBS), incubated in PBS containing 0.01 mg mL^{-1} S4B (Anderson et al., 2010) for 30 min, and rinsed in PBS. All fully expanded leaves (12–20) were cut from each gametophore and mounted in PBS. Fluorescence images of each leaf, centered on the brightest part of the midrib, were captured using a Zeiss Axio Imager M2 with 43HE DsRed filter set, Plan-Neofluar 20×/0.5 objective, AxioCam MR R3 camera, and Zen Blue software, version 1.1.2.0 (Carl Zeiss Microscopy), under identical conditions using manual exposure. The midrib in each image was selected manually (Supplemental Fig. S10), and average pixel intensity was measured using ImageJ, Fiji version (Schindelin et al., 2012). For comparison of KOs with the wild type, three independent lines of each KO genotype (n = 3) and two independent wild type lines (GD06 and GD11; n = 2) were sampled in triplicate. For analysis of rescue lines, three independent explants were sampled for each genetic line (n = 3).

For affinity cytochemistry of cellulose, gametophores dissected from colonies grown for 2 weeks on BCDAT medium were fixed and embedded in LR White resin (Polysciences) as described previously (Kulkarni et al., 2012). Sections (1 μm) were mounted and labeled with CBM3a as described previously (Berry et al., 2016). Images were captured with a Zeiss Axio Imager M2 with 38 GFP

filter set, EC Plan-Neofluar 40×/0.75 objective, AxioCam MR R3 camera, and Zen Blue software, version 1.1.2.0 (Carl Zeiss Microscopy), under identical conditions using manual exposure. Fluorescence and polarization images were not altered after capture. Bright-field and differential interference contrast images were captured using automatic exposure, and some images used for illustrative purposes were adjusted for uniformity using the color-balance and exposure functions in Photoshop, version CS6 (Adobe Systems).

*ppcesa3*KOs, *ppcesa8*KOs, and *ppcesa3/8*KOs were tested for changes in caulonema gravitropism and rhizoid development as described previously (Roberts et al., 2011). Images were captured using a Leica M165FC stereomicroscope with Leica DFC310FX camera and Leica Application Suite software, version 4.2.0 (Leica Microsystems). Caulonema length for each colony was measured as the distance from the edge of the colony to the tip of the longest caulonema filament using Leica Application Suite software.

Cell Wall Analysis

Alcohol-insoluble residue was prepared from gametophores dissected from eight to 10 4-week-old explants of *P. patens* wild type (three samples from independent cultures) and *ppcesa3/8*KO (samples from three independent lines) cultured on BCDAT medium. Tissue was ground in liquid nitrogen and extracted three times, 30 min each, with 70% (v/v) ethanol and once with 100% ethanol, and the residue was dried under vacuum. The alcohol-insoluble residue (~1 mg) was weighed to 0.001 mg and mixed with 1 mL of acetic acid:water:nitric acid (8:2:1, v/v) in screw-cap vials, and the suspension was heated in a boiling water bath for 30 min (Updegraff, 1969). After cooling, the tubes were centrifuged at 16,900*g* for 5 min and the supernatant was discarded. The pellet was resuspended in 2 mL of deionized water and centrifuged, and the supernatant was discarded. The washing step was repeated at least 10 more times until the supernatant was neutralized, and the pellet was resuspended in 1 mL of water. The amount of cellulose remaining after hydrolysis was quantified by sulfuric acid assay (Albalasmeh et al., 2013) with Glc as the standard. Briefly, 100 μL of hydrolysate (six technical replicates per sample) was diluted to 1 mL with water in a glass tube, 3 mL of concentrated sulfuric acid was added, and samples were vortexed for 30 s and chilled on ice for 2 min. Reactions were measured at 315 nm against a reagent blank.

High-Pressure Freezing-Freeze Substitution and Transmission Electron Microscopy

Gametophytes of *P. patens* GD06 and PpCESAKOs were high-pressure frozen using a Leica EMPACT2 high-pressure freezer (Leica Microsystems) followed by freeze substitution in 0.1% uranyl acetate (w/v) in acetone for 48 h at −90°C before the temperature was ramped up slowly to −50°C (Wilson and Bacic, 2012). The samples were rinsed with acetone twice at −50°C before the acetone was replaced with ethanol, and the samples were subsequently infiltrated with LR White resin (ProSciTech) in a series of ethanol/resin dilutions. The samples were rinsed three times in 100% resin before polymerization with UV light at −20°C for 48 h. Thin sections (70 nm) were cut using a Leica Ultracut R (Leica Microsystems) and poststained with uranyl acetate and lead citrate (Wilson and Bacic, 2012). Images were taken using a Tecnai G2 Spirit transmission electron microscope (FEI). Cell wall thickness was measured using ImageJ, Fiji version (Schindelin et al., 2012).

Ultrathin sections (70 nm) also were cut from blocks prepared for affinity cytochemistry (see above), mounted on formvar-coated copper grids, and stained with uranyl acetate and lead citrate (Wilson and Bacic 2012). Sections were imaged using a FEI/Phillips CM-200 transmission electron microscope (FEI).

SFG Spectroscopy

Leaves of wild type GD06, 8KO-5B, and 3/8KO-86 lines were mounted abaxial side down in water on glass slides and allowed to air dry overnight. SFG spectra were collected in 5-μm intervals along a 200-μm line scan perpendicular to the midrib at its thickest point using an SFG microscope system described previously (Lee et al., 2016). The SFG spectra were collected with the following polarization combination: SFG signal = s-, 800 nm = s-, and broadband mid-IR = p-polarized with the laser incidence plane and the laser incidence plane aligned along the axis of midrib.

Reverse Transcription Quantitative PCR

RNA was extracted from gametophores from two independent wild type and three independent lines each of *ppcesa3*KO and *ppcesa8*KO as described previously (Tran and Roberts, 2016). cDNA samples were tested in duplicate as described previously using primer pairs for the amplification of *PpCESA3* and *PpCESA8*. The primers were tested previously for specificity and efficiency (Tran and Roberts, 2016). Primers for actin and v-type H^+-translocating pyrophosphatase reference genes were described previously (Le Bail et al., 2013). Target/average reference cross-point ratios were calculated for each sample, and SE values were calculated for independent genetic lines.

Statistical Analysis

For statistical analysis, one-way ANOVA with posthoc Tukey's Honestly Significant Difference test was performed at astatsa.com/OneWay_Anova_with_TukeyHSD/.

Accession Numbers

Sequence data from this article can be found in the GenBank/EMBL data libraries under accession numbers DQ902545, DQ902546, DQ902549, DQ160224, DQ160225, XP_001753310, and XP_001776974.

Supplemental Data

The following supplemental materials are available.

Supplemental Figure S1. Genotype analysis of *ppcesa8*KO, *ppcesa3*KO, and *ppcesa3/8*KO lines.

Supplemental Figure S2. Phenotype analysis of a *ppcesa3/8*KO line transformed with vectors driving the expression of *PpCESA3* or *PpCESA8* with their native promoters.

Supplemental Figure S3. Transmission electron microscopy images of leaf cell walls from wild type and *cesa*KO lines of *P. patens*.

Supplemental Figure S4. Thickness of outer cell walls measured from transmission electron microscopy images.

Supplemental Figure S5. *P. patens* wild type and KO lines cultured on medium containing 1 μM naphthalene acetic acid to induce rhizoid initiation and inhibit leaf initiation.

Supplemental Figure S6. *P. patens* wild type and KO lines cultured in the dark on vertically oriented plates containing medium supplemented with 35 mM Suc to test for caulonema gravitropism.

Supplemental Figure S7. Western-blot analysis of protein expression for *P. patens* lines derived from the transformation of *ppcesa3/8*KO-86lox with vectors driving the expression of PpCESAs under the control of the *PpCESA8* promoter.

Supplemental Figure S8. PCR-based genotyping of *ppcesa6/7*KO lines.

Supplemental Figure S9. PCR-based genotyping of *ppcesa4/10*KO lines.

Supplemental Figure S10. Quantification method for S4B fluorescence.

Supplemental Table S1. Primers used for vector construction and genotype analysis.

ACKNOWLEDGMENTS

Clones pdp39044 and pdp10281 were from RIKEN BRC; we thank Chessa Goss and Virginia Lai for preliminary work on *ppceas8*KO, Alfred Schupp for assistance with vector construction, Evan Preisser for assistance with statistics, and Sarah Kiemle for conducting Updegraff assays.

Received July 6, 2017; accepted July 24, 2017; published August 2, 2017.

LITERATURE CITED

Albalasmeh AA, Berhe AA, Ghezzehei TA (2013) A new method for rapid determination of carbohydrate and total carbon concentrations using UV spectrophotometry. Carbohydr Polym **97:** 253–261

Anderson CT, Carroll A, Akhmetova L, Somerville C (2010) Real-time imaging of cellulose reorientation during cell wall expansion in Arabidopsis roots. Plant Physiol **152:** 787–796

Barnett JR, Bonham VA (2004) Cellulose microfibril angle in the cell wall of wood fibres. Biol Rev Camb Philos Soc **79:** 461–472

Barnette AL, Bradley LC, Veres BD, Schreiner EP, Park YB, Park J, Park S, Kim SH (2011) Selective detection of crystalline cellulose in plant cell walls with sum-frequency-generation (SFG) vibration spectroscopy. Biomacromolecules **12:** 2434–2439

Barnette AL, Lee C, Bradley LC, Schreiner EP, Park YB, Shin H, Cosgrove DJ, Park S, Kim SH (2012) Quantification of crystalline cellulose in lignocellulosic biomass using sum frequency generation (SFG) vibration spectroscopy and comparison with other analytical methods. Carbohydr Polym **89:** 802–809

Berry EA, Tran ML, Dimos CS, Budziszek MJ Jr, Scavuzzo-Duggan TR, Roberts AW (2016) Immuno and affinity cytochemical analysis of cell wall composition in the moss *Physcomitrella patens*. Front Plant Sci **7:** 248

Betancur L, Singh B, Rapp RA, Wendel JF, Marks MD, Roberts AW, Haigler CH (2010) Phylogenetically distinct cellulose synthase genes support secondary wall thickening in Arabidopsis shoot trichomes and cotton fiber. J Integr Plant Biol **52:** 205–220

Blake AW, McCartney L, Flint JE, Bolam DN, Boraston AB, Gilbert HJ, Knox JP (2006) Understanding the biological rationale for the diversity of cellulose-directed carbohydrate-binding modules in prokaryotic enzymes. J Biol Chem **281:** 29321–29329

Carafa A, Duckett JG, Knox JP, Ligrone R (2005) Distribution of cell-wall xylans in bryophytes and tracheophytes: new insights into basal interrelationships of land plants. New Phytol **168:** 231–240

Carpita N, McCann M (2000) The cell wall. *In* B Buchanan, W Gruissem, R Jones, eds, Biochemistry and Molecular Biology of Plants. American Society of Plant Physiologists, Rockville, MD, pp 52–108

Carroll A, Mansoori N, Li S, Lei L, Vernhettes S, Visser RG, Somerville C, Gu Y, Trindade LM (2012) Complexes with mixed primary and secondary cellulose synthases are functional in Arabidopsis plants. Plant Physiol **160:** 726–737

Delmer DP (1999) Cellulose biosynthesis: exciting times for a difficult field of study. Annu Rev Plant Physiol Plant Mol Biol **50:** 245–276

Desprez T, Juraniec M, Crowell EF, Jouy H, Pochylova Z, Parcy F, Höfte H, Gonneau M, Vernhettes S (2007) Organization of cellulose synthase complexes involved in primary cell wall synthesis in Arabidopsis thaliana. Proc Natl Acad Sci USA **104:** 15572–15577

Donaldson L (2007) Cellulose microfibril aggregates and their size variation with cell wall type. Wood Sci Technol **41:** 443–460

Emons AMC, Mulder BM (2000) How the deposition of cellulose microfibrils builds cell wall architecture. Trends Plant Sci **5:** 35–40

Fernandes AN, Thomas LH, Altaner CM, Callow P, Forsyth VT, Apperley DC, Kennedy CJ, Jarvis MC (2011) Nanostructure of cellulose microfibrils in spruce wood. Proc Natl Acad Sci USA **108:** E1195–E1203

Gonneau M, Desprez T, Guillot A, Vernhettes S, Höfte H (2014) Catalytic subunit stoichiometry within the cellulose synthase complex. Plant Physiol **166:** 1709–1712

Goss CA, Brockmann DJ, Bushoven JT, Roberts AW (2012) A *CELLULOSE SYNTHASE* (*CESA*) gene essential for gametophore morphogenesis in the moss *Physcomitrella patens*. Planta **235:** 1355–1367

Haigler CH, Betancur L, Stiff MR, Tuttle JR (2012) Cotton fiber: a powerful single-cell model for cell wall and cellulose research. Front Plant Sci **3:** 104

Hebant C (1977) The Conducting Tissues of Bryophytes. J. Cramer, Vaduz, Liechtenstein

Hill JL Jr, Hammudi MB, Tien M (2014) The *Arabidopsis* cellulose synthase complex: a proposed hexamer of CESA trimers in an equimolar stoichiometry. Plant Cell **26:** 4834–4842

Jarvis MC (2013) Cellulose biosynthesis: counting the chains. Plant Physiol **163:** 1485–1486

Kenrick P, Crane PR (1997) The origin and early evolution of plants on land. Nature **389:** 33–39

Kimura S, Laosinchai W, Itoh T, Cui X, Linder CR, Brown RM Jr (1999) Immunogold labeling of rosette terminal cellulose-synthesizing complexes in the vascular plant *Vigna angularis*. Plant Cell **11:** 2075–2086

Kulkarni AR, Peña MJ, Avci U, Mazumder K, Urbanowicz BR, Pattathil S, Yin Y, O'Neill MA, Roberts AW, Hahn MG, et al (2012) The ability of land plants to synthesize glucuronoxylans predates the evolution of tracheophytes. Glycobiology **22:** 439–451

Kumar M, Atanassov I, Turner S (2017) Functional analysis of cellulose synthase (CESA) protein class specificity. Plant Physiol **173:** 970–983

Le Bail A, Scholz S, Kost B (2013) Evaluation of reference genes for RT qPCR analyses of structure-specific and hormone regulated gene expression in *Physcomitrella patens* gametophytes. PLoS ONE **8:** e70998

Lee CM, Kafle K, Huang S, Kim SH (2016) Multimodal broadband vibrational sum frequency generation (MM-BB-V-SFG) spectrometer and microscope. J Phys Chem B **120:** 102–116

Lee CM, Kafle K, Park YB, Kim SH (2014) Probing crystal structure and mesoscale assembly of cellulose microfibrils in plant cell walls, tunicate tests, and bacterial films using vibrational sum frequency generation (SFG) spectroscopy. Phys Chem Chem Phys **16:** 10844–10853

Ligrone R, Vaughn KC, Renzaglia KS, Knox JP, Duckett JG (2002) Diversity in the distribution of polysaccharide and glycoprotein epitopes in the cell walls of bryophytes: new evidence for the multiple evolution of water-conducting cells. New Phytol **156:** 491–508

Lindeboom J, Mulder BM, Vos JW, Ketelaar T, Emons AM (2008) Cellulose microfibril deposition: coordinated activity at the plant plasma membrane. J Microsc **231:** 192–200

Newman RH, Hill SJ, Harris PJ (2013) Wide-angle x-ray scattering and solid-state nuclear magnetic resonance data combined to test models for cellulose microfibrils in mung bean cell walls. Plant Physiol **163:** 1558–1567

Nixon BT, Mansouri K, Singh A, Du J, Davis JK, Lee JG, Slabaugh E, Vandavasi VG, O'Neill H, Roberts EM, et al (2016) Comparative structural and computational analysis supports eighteen cellulose synthases in the plant cellulose synthesis complex. Sci Rep **6:** 28696

Oehme DP, Downton MT, Doblin MS, Wagner J, Gidley MJ, Bacic A (2015) Unique aspects of the structure and dynamics of elementary Iβ cellulose microfibrils revealed by computational simulations. Plant Physiol **168:** 3–17

Park YB, Lee CM, Koo BW, Park S, Cosgrove DJ, Kim SH (2013) Monitoring meso-scale ordering of cellulose in intact plant cell walls using sum frequency generation spectroscopy. Plant Physiol **163:** 907–913

Persson S, Paredez A, Carroll A, Palsdottir H, Doblin M, Poindexter P, Khitrov N, Auer M, Somerville CR (2007) Genetic evidence for three unique components in primary cell-wall cellulose synthase complexes in Arabidopsis. Proc Natl Acad Sci USA **104:** 15566–15571

Rensing SA, Lang D, Zimmer AD, Terry A, Salamov A, Shapiro H, Nishiyama T, Perroud PF, Lindquist EA, Kamisugi Y, et al (2008) The *Physcomitrella* genome reveals evolutionary insights into the conquest of land by plants. Science **319:** 64–69

Roberts AW, Bushoven JT (2007) The cellulose synthase (*CESA*) gene superfamily of the moss *Physcomitrella patens*. Plant Mol Biol **63:** 207–219

Roberts AW, Dimos CS, Budziszek MJ Jr, Goss CA, Lai V (2011) Knocking out the wall: protocols for gene targeting in *Physcomitrella patens*. Methods Mol Biol **715:** 273–290

Roberts AW, Roberts EM, Haigler CH (2012) Moss cell walls: structure and biosynthesis. Front Plant Sci **3:** 166

Scavuzzo-Duggan TR, Chaves AM, Roberts AW (2015) A complementation assay for in vivo protein structure/function analysis in *Physcomitrella patens* (Funariaceae). Appl Plant Sci **3:** 1500023

Schaefer DG, Zrÿd JP (1997) Efficient gene targeting in the moss *Physcomitrella patens*. Plant J **11:** 1195–1206

Schindelin J, Arganda-Carreras I, Frise E, Kaynig V, Longair M, Pietzsch T, Preibisch S, Rueden C, Saalfeld S, Schmid B, et al (2012) Fiji: an open-source platform for biological-image analysis. Nat Methods **9:** 676–682

Schuetz M, Smith R, Ellis B (2013) Xylem tissue specification, patterning, and differentiation mechanisms. J Exp Bot **64:** 11–31

Shen H, Yin Y, Chen F, Xu Y, Dixon RA (2009) A bioinformatic analysis of NAC genes for plant cell wall development in relation to lignocellulosic bioenergy production. Bioenerg Res **2:** 217–232

Taylor JG, Owen TP Jr, Koonce LT, Haigler CH (1992) Dispersed lignin in tracheary elements treated with cellulose synthesis inhibitors provides evidence that molecules of the secondary cell wall mediate wall patterning. Plant J **2:** 959–970

Taylor NG, Gardiner JC, Whiteman R, Turner SR (2004) Cellulose synthesis in the Arabidopsis secondary cell wall. Cellulose **11:** 329–338

Taylor NG, Howells RM, Huttly AK, Vickers K, Turner SR (2003) Interactions among three distinct CesA proteins essential for cellulose synthesis. Proc Natl Acad Sci USA **100:** 1450–1455

Taylor NG, Laurie S, Turner SR (2000) Multiple cellulose synthase catalytic subunits are required for cellulose synthesis in *Arabidopsis*. Plant Cell **12:** 2529–2540

Thomas LH, Forsyth VT, Martel A, Grillo I, Altaner CM, Jarvis MC (2014) Structure and spacing of cellulose microfibrils in woody cell walls of dicots. Cellulose **21:** 3887–3895

Timmers J, Vernhettes S, Desprez T, Vincken JP, Visser RG, Trindade LM (2009) Interactions between membrane-bound cellulose synthases involved in the synthesis of the secondary cell wall. FEBS Lett **583:** 978–982

Tran ML, Roberts AW (2016) Cellulose synthase gene expression profiling of Physcomitrella patens. Plant Biol (Stuttg) **18:** 362–368

Updegraff DM (1969) Semimicro determination of cellulose in biological materials. Anal Biochem **32:** 420–424

Vandavasi VG, Putnam DK, Zhang Q, Petridis L, Heller WT, Nixon BT, Haigler CH, Kalluri U, Coates L, Langan P, et al (2016) A structural study of CESA1 catalytic domain of Arabidopsis cellulose synthesis complex: evidence for CESA trimers. Plant Physiol **170:** 123–135

Vidali L, Burkart GM, Augustine RC, Kerdavid E, Tüzel E, Bezanilla M (2010) Myosin XI is essential for tip growth in *Physcomitrella patens*. Plant Cell **22:** 1868–1882

Vidali L, van Gisbergen PA, Guérin C, Franco P, Li M, Burkart GM, Augustine RC, Blanchoin L, Bezanilla M (2009) Rapid formin-mediated actin-filament elongation is essential for polarized plant cell growth. Proc Natl Acad Sci USA **106:** 13341–13346

Wilson SM, Bacic A (2012) Preparation of plant cells for transmission electron microscopy to optimize immunogold labeling of carbohydrate and protein epitopes. Nat Protoc **7:** 1716–1727

Wise HZ, Saxena IM, Brown RM Jr (2011) Isolation and characterization of the cellulose synthase genes *PpCesA6* and *PpCesA7* in *Physcomitrella patens*. Cellulose **18:** 371–384

Xu B, Ohtani M, Yamaguchi M, Toyooka K, Wakazaki M, Sato M, Kubo M, Nakano Y, Sano R, Hiwatashi Y, et al (2014) Contribution of NAC transcription factors to plant adaptation to land. Science **343:** 1505–1508

Yang JH, Wang H (2016) Molecular mechanisms for vascular development and secondary cell wall formation. Front Plant Sci **7:** 356

Yin Y, Huang J, Xu Y (2009) The cellulose synthase superfamily in fully sequenced plants and algae. BMC Plant Biol **9:** 99

Zhong R, Ye ZH (2015) Secondary cell walls: biosynthesis, patterned deposition and transcriptional regulation. Plant Cell Physiol **56:** 195–214

Zhu T, Nevo E, Sun D, Peng J (2012) Phylogenetic analyses unravel the evolutionary history of NAC proteins in plants. Evolution **66:** 1833–1848